NeuroImage 232 (2021) 117898

Contents lists available at ScienceDirect

NeuroImage

journal homepage: www.elsevier.com/locate/neuroimage

Abnormal meta-state activation of dynamic brain networks across the Alzheimer spectrum

Pablo Núñez[a,*], Jesús Poza[a,b,c], Carlos Gómez[a,b], Víctor Rodríguez-González[a], Arjan Hillebrand[d], Prejaas Tewarie[d], Miguel Ángel Tola-Arribas[b], Mónica Cano[e], Roberto Hornero[a,b,c]

[a] Biomedical Engineering Group, University of Valladolid, Valladolid, Spain
[b] Centro de Investigación Biomédica en Red en Bioingeniería, Biomateriales y Nanomedicina, (CIBER-BBN), Madrid, Spain
[c] IMUVA, Instituto de Investigación en Matemáticas, University of Valladolid, Spain
[d] Department of Clinical Neurophysiology and MEG Center, Amsterdam UMC, Vrije Universiteit Amsterdam, Amsterdam Neuroscience, Amsterdam, The Netherlands
[e] Department of Clinical Neurophysiology, "Río Hortega" University Hospital, Valladolid, Spain

ARTICLE INFO

Keywords:
Dynamic functional connectivity
Dementia due to Alzheimer's disease
Mild cognitive impairment
Electroencephalography
Instantaneous amplitude correlation
Community detection

ABSTRACT

The characterization of the distinct dynamic functional connectivity (dFC) patterns that activate in the brain during rest can help to understand the underlying time-varying network organization. The presence and behavior of these patterns (known as meta-states) have been widely studied by means of functional magnetic resonance imaging (fMRI). However, modalities with high-temporal resolution, such as electroencephalography (EEG), enable the characterization of fast temporally evolving meta-state sequences. Mild cognitive impairment (MCI) and dementia due to Alzheimer's disease (AD) have been shown to disrupt spatially localized activation and dFC between different brain regions, but not much is known about how they affect meta-state network topologies and their network dynamics. The main hypothesis of the study was that MCI and dementia due to AD alter normal meta-state sequences by inducing a loss of structure in their patterns and a reduction of their dynamics. Moreover, we expected that patients with MCI would display more flexible behavior compared to patients with dementia due to AD. Thus, the aim of the current study was twofold: (i) to find repeating, distinctly organized network patterns (meta-states) in neural activity; and (ii) to extract information about meta-state fluctuations and how they are influenced by MCI and dementia due to AD. To accomplish these goals, we present a novel methodology to characterize dynamic meta-states and their temporal fluctuations by capturing aspects based on both their discrete activation and the continuous evolution of their individual strength. These properties were extracted from 60-s resting-state EEG recordings from 67 patients with MCI due to AD, 50 patients with dementia due to AD, and 43 cognitively healthy controls. First, the instantaneous amplitude correlation (IAC) was used to estimate instantaneous functional connectivity with a high temporal resolution. We then extracted meta-states by means of graph community detection based on recurrence plots (RPs), both at the individual- and group-level. Subsequently, a diverse set of properties of the continuous and discrete fluctuation patterns of the meta-states was extracted and analyzed. The main novelty of the methodology lies in the usage of Louvain GJA community detection to extract meta-states from IAC-derived RPs and the extended analysis of their discrete and continuous activation. Our findings showed that distinct dynamic functional connectivity meta-states can be found on the EEG time-scale, and that these were not affected by the oscillatory slowing induced by MCI or dementia due to AD. However, both conditions displayed a loss of meta-state modularity, coupled with shorter dwell times and higher complexity of the meta-state sequences. Furthermore, we found evidence that meta-state sequencing is not entirely random; it shows an underlying structure that is partially lost in MCI and dementia due to AD. These results show evidence that AD progression is associated with alterations in meta-state switching, and a degradation of dynamic brain flexibility.

1. Introduction

The human brain is a complex system comprised of a vast network of neurons connected by synapses that engage in continuous ongoing electrical and chemical processes that appear and dissolve across multiple spatial and temporal scales (Babiloni et al., 2016b; Tognoli and Kelso, 2014). A large body of work has studied the functional interac-

* Corresponding author.
E-mail address: pablo.nunez@gib.tel.uva.es (P. Núñez).

https://doi.org/10.1016/j.neuroimage.2021.117898
Received 8 October 2020; Received in revised form 19 January 2021; Accepted 16 February 2021
Available online 20 February 2021

tions (functional connectivity, FC) between these neuronal ensembles in a strictly static sense, overlooking the possible temporal dimensions at play in these interactions (O'Neill et al., 2018). This field, known as *static functional connectivity* (sFC), assumes that the statistical interdependence between brain regions remains temporally stationary during the resting-state (Hindriks et al., 2016). While studies on sFC have offered significant insights into the properties of neural activity (Hutchison et al., 2013), it has been shown that the brain does not remain in a state of static equilibrium. Instead, it undergoes complex dynamic behavior with patterns of FC that fluctuate in time and space (Hansen et al., 2015; O'Neill et al., 2018). Hence, it has been proposed that resting-state networks display meaningful dynamic behavior that is also distinct from the one found in task-driven brain activity (Deco et al., 2013). This novel field, known as *dynamic functional connectivity* (dFC), has opened the gates to a large array of studies that aim to look past previous assumptions of stationarity during rest (for reviews, see Deco et al. (2013); O'Neill et al. (2018)).

Neuronal activity can be measured with different techniques, such as functional magnetic resonance imaging (fMRI), electroencephalography (EEG) and magnetoencephalography (MEG). Each of these techniques is useful to estimate neuronal interactions at different temporal and spatial scales, such as on the order of seconds to minutes (fMRI) and milliseconds (MEG and EEG) (Núñez et al., 2019a; Tewarie et al., 2019). While most dFC research has been conducted using fMRI, its time-varying behavior evolves at a very slow rate and is not able to characterize the potentially fast neuronal dynamics (O'Neill et al., 2018). In contrast, the high temporal resolution of both MEG and EEG allows for a precise measurement of the (dynamically changing) oscillations that lie at the core of brain function (Babiloni et al., 2016b; O'Neill et al., 2018). While MEG provides a higher spatial resolution, EEG is a cost-effective technique, widely used in clinical settings, that directly measures the electrical activity generated by postsynaptic potentials (Núñez et al., 2019a; Poza et al., 2017).

Even though neurophysiological techniques enable the detection of very fast dynamics of functional interaction, most traditional EEG/MEG dFC studies suffer from the limitation of being based on sliding windows (segments of a relatively large number of temporal samples) from which the FC is estimated (Fraschini et al., 2016; O'Neill et al., 2018; Tewarie et al., 2019). The sliding window approach suffers from a series of limitations, such as the necessity of choosing a non-trivial window size (Fraschini et al., 2016; Liuzzi et al., 2019; Núñez et al., 2019a). In this study we used a recently proposed measure of very high resolution FC: the instantaneous amplitude correlation (IAC) (Tewarie et al., 2019). In order to account for the high susceptibility to noise of this metric, a compromise between traditional sliding windows and instantaneous FC can be reached by means of data-driven windows based on recurrence plots (RPs), (Tewarie et al., 2019), which are two-dimensional symmetric matrices that represent visits to the same area in the phase space of a dynamical system (Deco et al., 2017b; Marwan et al., 2007; Webber and Zbilut, 2005).

Here, we advance the methodology presented by Tewarie et al. (2019) by using these RPs to estimate the time windows in which the system can be considered to be in the same state, and extracting temporally repeating FC patterns by means of community detection methods (Bassett et al., 2013; O'Neill et al., 2018). In this study, we propose to extract these patterns by means of a community detection algorithm (Louvain GJA) that does not require *a priori* definition of the number of meta-states (Zhou et al., 2019). This is a known limitation of most methods for the identification of repeating connectivity patterns, such as *k*-means clustering (O'Neill et al., 2018). These communities can be interpreted as temporally repeating brain network configurations (meta-states). After extracting temporally repeating meta-states, we construct a summary of the temporal activation of these states, and extract relevant information about the underlying temporal structure of the functional brain networks. In order to achieve a comprehensive and novel characterization of brain dynamics, we computed two types of metrics: (i) based on the discrete temporal activation of the meta-states, and (ii) based on the continuous correlation of each meta-state with the instantaneous FC. This new methodology provides new information on brain meta-state switching that can be used to investigate the possible alterations to normal brain behavior during rest that may be induced by neurological disorders.

To assess the ability of this new methodology to detect meaningful information, we apply it to two closely related conditions that affect brain activity: mild cognitive impairment (MCI) and dementia due to Alzheimer's disease (AD). Dementia due to AD is a neurodegenerative disorder that has been shown to perturb EEG brain activity. AD is characterized by the progressive disruption of different brain areas (Palop and Mucke, 2010; Pievani et al., 2011). Some observed disruptions include power shifts of neural activity to lower frequencies, aberrant connectivity patterns, and alterations of network properties (Rossini et al., 2020). MCI is sometimes considered a prodromal stage of AD, with both disorders being seen as part of the same continuum (Petersen, 2004). We found that patients with MCI often show subtle neural abnormalities compared to normal aging than can be seen as an early indicator of AD (Poza et al., 2017). In our previous studies we observed these effects that pointed to frequency-dependent aberrant dynamic behavior in MCI and dementia due to AD (Núñez et al., 2020; 2019b). Patients with MCI and dementia due to AD displayed abnormal electrode-level EEG activity recurrence and non-stationarity patterns. Specifically, controls showed higher levels of non-stationarity compared to MCI and AD in the theta and alpha bands; the opposite behavior occurred in the beta band, pointing to aberrant state switching in MCI and AD (Núñez et al., 2020). We also found a significant reduction in alpha and beta amplitude envelope correlation dFC (using sliding windows) in AD compared to controls, indicating a loss of neural dynamics in patients with this condition (Núñez et al., 2019b).

Based on these premises, in the present study, we hypothesized that MCI and dementia due to AD might alter normal meta-state sequencing, inducing a loss of underlying structure of repeating patterns in said sequences, as well as a loss in dynamics of general state fluctuations. Consequently, the purpose of the present study is twofold: (i) in a first step, we focused on finding stable, distinctly organized repeating network patterns (meta-states); and (ii) secondly, we aimed at extracting relevant information about the fluctuations of these meta-states to study how they are influenced by MCI and dementia due to AD. The manuscript is structured in two parts: first, a novel methodology for meta-state extraction by means of a RP and community detection is presented; then, the extracted meta-states, their temporal sequencing, and dynamical properties are compared between healthy controls, patients with MCI and patients with dementia due to AD.

2. Materials

2.1. Subjects

The study sample was formed by 160 subjects: 43 cognitively healthy controls, 67 patients with MCI due to AD, and 50 patients with dementia due to AD. The criteria of the National Institute on Aging and Alzheimer's Association (NIA-AA) were used to diagnose the patients with MCI or dementia due to AD (Albert et al., 2011; McKhann et al., 2011). The control group was composed of elderly subjects with no history of neurological or psychiatric disorders. Potential participants were excluded according to the following exclusion criteria: (1) presence or history of other neurological or psychiatric diseases; (2) atypical course or uncommon clinical presentations according to the NIA-AA criteria;

Table 1
Socio-demographic and clinical data. AD: Alzheimer's disease; MCI: mild cognitive impairment; m: median; IQR: interquartile range ; M: male; F: female; A: primary education or below; B: secondary education or above; MMSE: Mini-Mental State Examination.

Data	Group		
	Patients with AD	Patients with MCI	Controls
Number of subjects	50	67	43
Age (years) (m[IQR])	78.5[75.7, 82.4]	77.2[72.2, 80.6]	75.8[74.0, 78.7]
Sex (M:F)	23 : 27	29 : 38	13 : 30
Education level (A:B)	35 : 15	41 : 26	16 : 27
MMSE (m[IQR])	22[20, 24]	27[26, 28]	29[28, 30]

(3) advanced dementia (Clinical Dementia Rating = 3); (4) institutionalized patients; or (5) medication that could have an influence on EEG activity. The socio-demographic characteristics of each group are specified in Table 1. The database used in this study is an updated version of the one used in Núñez et al. (2019b) and Núñez et al. (2020).

Statistical analyses were conducted over all clinical and socio-demographic data in order to assess possible differences between groups that may act as confounding factors. The groups did not differ in age ($\chi^2(2) = 4.62$, $p = .091$, Kruskal-Wallis test) or sex ($\chi^2(2) = 2.72$, $p = .256$, Chi-squared test). The groups did show statistically significant differences in education level ($\chi^2(2) = 10.81$, $p < .001$, Chi-squared test). Thus, statistical differences between both education levels were assessed for all the extracted measures (see Section 4.2).

As expected, MMSE scores were lower in patients with AD compared to controls ($U = 8.184$, $p < .001$, Mann-Whitney U-test) and patients with MCI ($U = 8.074$, $p < .001$, Mann-Whitney U-test). MMSE scores were also lower in patients with MCI compared to controls ($U = 5.463$, $p < .001$, Mann-Whitney U-test).

All participants and caregivers were informed about the research and study protocol and gave their written informed consent. The Ethics Committee of the "Río Hortega" University Hospital (Valladolid, Spain) approved the study (36/2014/02) according to the Code of Ethics of the World Medical Association (Declaration of Helsinki).

2.2. Electroencephalographic recordings

EEG signals were recorded by means of a 19-channel EEG system (XLTEK®, Natus Medical) at the Department of Clinical Neurophysiology of the "Río Hortega" University Hospital, Valladolid, Spain. EEG activity was recorded from electrodes Fp1, Fp2, Fz, F3, F4, F7, F8, Cz, C3, C4, T3, T4, T5, T6, Pz, P3, P4, O1, and O2, according to the specifications of the international 10–20 system and at a sampling frequency of 200 Hz. The recorded signals were bipolar and re-referenced by means of common average referencing (CAR) (Núñez et al., 2019a). Subjects were asked to remain awake, still, and with eyes closed during the acquisition of the EEG. In order to prevent sleepiness, EEG traces were visually monitored in real time. Drowsiness episodes, subtle muscle activity, and eye-movement related artifacts were identified and marked during the course of the EEG acquisition.

Five minutes of EEG activity were recorded for each subject. The EEG signals were then preprocessed in three steps (Núñez et al., 2020; 2019b): (i) independent component analysis to remove components with artifacts, such as the heartbeat, eye blinks and electromyographic artifacts; (ii) finite impulse response (FIR) filtering (Hamming window, filter order 2000, forward and backward filtering) to remove 50 Hz noise and to limit spectral content to the wide frequency band of [1 70] Hz; and (iii) visual rejection of any remaining artifacts, selecting the first 60 consecutive seconds of artifact-free activity for each subject.

3. Methods

3.1. Source localization: Sloreta

The EEG time series were reconstructed at the source level by means of standardized low resolution brain electromagnetic tomography (sLORETA), which estimates a specific solution to the EEG inverse problem with zero localization errors (Pascual-Marqui, 2002). Localization inference in sLORETA is based on the standardization of the current density estimates (Pascual-Marqui, 2002). A sLORETA implementation is freely available in Brainstorm (http://neuroimage.usc.edu/brainstorm) (Tadel et al., 2011) and is described in detail in (Pascual-Marqui, 2002). This method has been widely used to analyze EEG activity (Babiloni et al., 2016a; Jatoi et al., 2014; Rodríguez-González et al., 2020).

A forward model was created using the anatomical information of the ICBM152 template from the Montreal Neurological Institute (Douw et al., 2018; Mazziotta et al., 2001). A three-layer head model (brain, skull, and scalp) was built using a Boundary Element method based on the aforementioned template using OpenMEEG software (Gramfort et al., 2010). This head model was used as source space, with a total number of 15,000 sources, which were restricted to be normal to cortex. The 15,000 source-reconstructed EEG time series were parcellated into the 68 cortical regions of interest (ROIs) of the Desikan-Killiany atlas by averaging the sources after flipping the sign of sources with opposite directions (Desikan et al., 2006).

Sign-flipping of sources over a ROI is performed due to an important limitation of sLORETA and other source reconstruction techniques, which is the fact that sources have arbitrary orientations (i.e., a source with a particular orientation will generate the same activation pattern at the electrode as one with the same orientation but opposite polarity) Vidaurre et al. (2016). This makes it impossible to distinguish between the two scenarios, as both would lead to the same EEG signal at the sensor level. For this reason, sign-flipping is necessary to avoid self-cancellation of neighboring sources when averaging over a region of interest (ROI), which would lead to distorted and incorrect reconstruction of averaged ROI activity.

3.2. Meta-state detection by means of community detection: Analysis steps

The analysis-steps of the study are visualized in Fig. 1. The workflow of the study was divided into four steps which are described in detail in the following sections. First **(1)**, an instantaneous FC tensor was computed by means of the IAC for all samples in the 60-s EEG recordings (68 ROIs × 68 ROIs × 12,000 samples). The IAC was computed in the conventional frequency bands: delta (δ, 1–4 Hz), theta (θ, 4–8 Hz), alpha (α, 8–13 Hz), beta-1 ($\beta 1$, 13–19 Hz), and beta-2 ($\beta 2$, 19–30 Hz). Then **(2)**, whole-recording RPs were computed from the IAC matrices of each temporal sample; and data-driven windows were obtained to mitigate the effect of noise and aggregate the data, as well as to reduce the size of the RPs for computational purposes. In the next step **(3a)**, in order to aggregate subject meta-states into generalized networks, per-group community detection was performed based on the RPs constructed from the data-driven windows of all subjects in a group. Afterwards **(3b)**, per-subject community detection was performed on the RPs of each subject. Finally **(4)**, two representations of the temporal evolution of the dominant subject-level meta-states were obtained. The first, called the *temporal activation sequence* (TAS), represents the discrete activation of the dominant meta-states. This was achieved by assigning each temporal sample in the time evolving FC tensor to the closest meta-state, in terms of the Spearman correlation. The second, the *instantaneous correlation tensor* (ICT) is a representation of the Spearman correlation of each meta-state with the IAC for each temporal sample. Then, a series of metrics, such as dwell time and complexity, were extracted from the TAS and the ICT.

The code for the computation of the IAC can be found on Github (https://github.com/Prejaas/

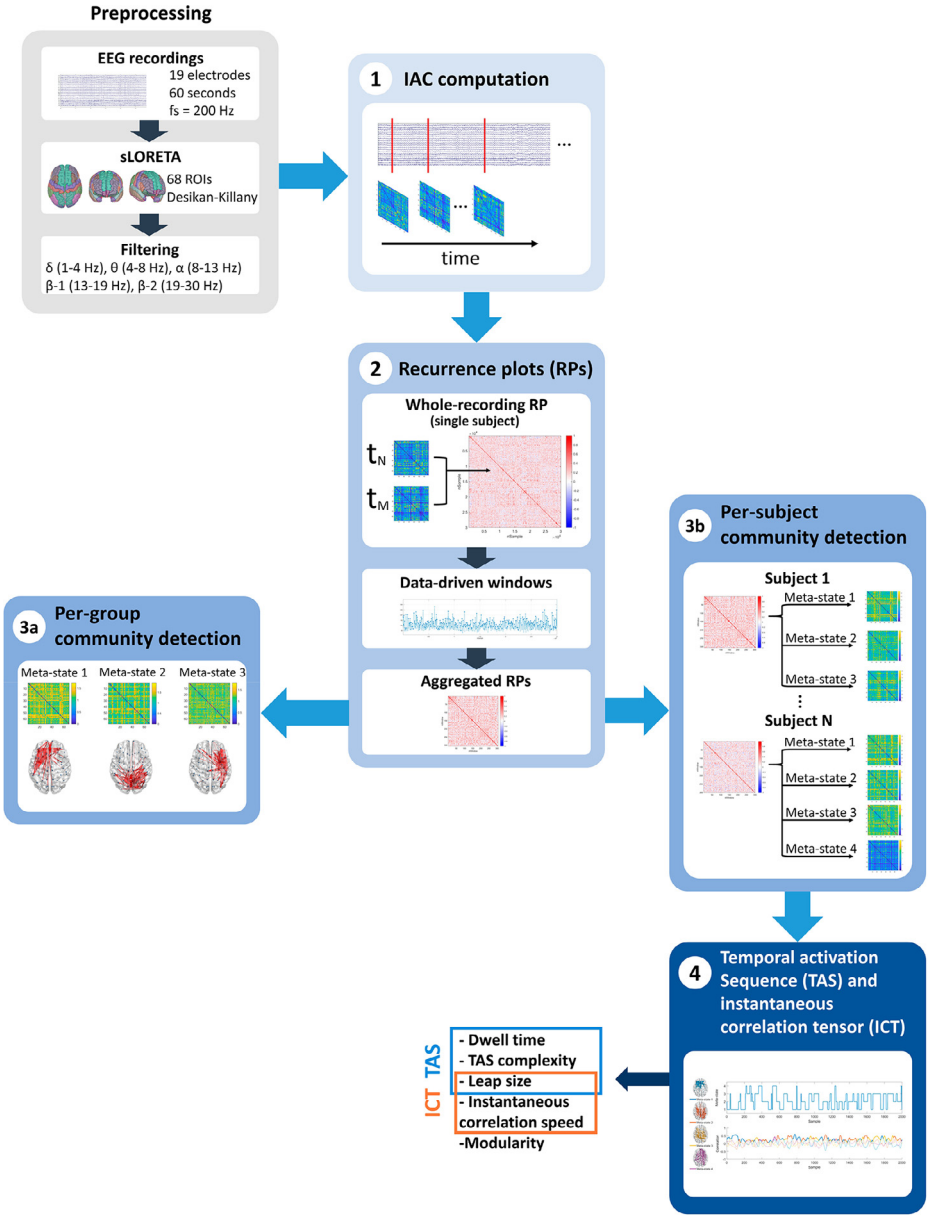

Fig. 1. Analysis-steps of the study. **(1)** Computation of instantaneous FC tensor by means of the IAC in the conventional frequency bands: delta (δ, 1–4 Hz), theta (θ, 4–8 Hz), alpha (α, 8–13 Hz), beta-1 ($\beta 1$, 13–19 Hz) and beta-2 ($\beta 2$, 19–30 Hz). **(2)** Computation of sample-by-sample whole-recording RPs from the IAC matrices, followed by identification of data-driven windows to mitigate the effect of noise and aggregate the data. Each sample corresponds to a sampling period of 5 ms. Each data-driven window has a duration of 5 ms × the specific number of samples in the window. **(3a)** Per-group community detection to aggregate subject meta-states into generalized networks. **(3b)** Per-subject community detection to extract distinct communities, identified as meta-states. **(4)** Computation of the *temporal activation sequence* (TAS) and the instantaneous correlation tensor (ICT), representing the discrete and continuous temporal evolution of the meta-states by means of their Spearman correlation with the instantaneous FC matrices. Computation of the modularity, as well as measures derived from the TAS (dwell time, TAS complexity), the ICS (instantaneous correlation speed), and from both (leap size).

High-temporal-resolution-MEG-measures-of-functional-connectivity). The code for the computation of data-driven windows, meta-state extraction, the TAS and ICT, and the metrics of meta-state activation can be found on Github as well (https://github.com/pablonuneznovo/Meta-state-extraction-from-high-temporal-resolution-connectivity).

3.2.1. *Instantaneous amplitude correlation (IAC)*

The *instantaneous amplitude correlation* (IAC) is a high temporal resolution measure of FC based on a widely used metric of static FC, *the amplitude envelope correlation* Brookes et al. (2011, 2014); O'Neill et al. (2015); it can be seen as its instantaneous counterpart (Tewarie et al., 2019). The IAC is based on the notion that if two regions display high amplitudes at the same time, their correlation will increase (Tewarie et al., 2019). Thus, the IAC is computed as the Hadamard product between the amplitude envelopes of two ROIs (Tewarie et al., 2019):

$$IAC_{ij}(t) = \hat{E}_i(t) \circ \hat{E}_j(t), \tag{1}$$

where $\circ$ represents the Hadamard product and $\hat{E}(t)$ is the amplitude envelope of a normalized (z-score) time-series. Due to its nature, the IAC is not sensitive to interactions due to negative correlations between the envelopes (Tewarie et al., 2019). In order to minimize spurious correlations due to the effects of spatial leakage, before the computation of the IAC, the time-series were pairwise orthogonalized after band-pass filtering (O'Neill et al., 2018).

3.2.2. *Recurrence plots (RPs) and data-driven windows*

The property of returning to previous states (recurrence) is a fundamental characteristic of many dynamical systems (Marwan et al., 2007). RPs are two-dimensional plots that can characterize the emergence and dissolution of states in dynamical systems and help to visualize periodicity patterns (Marwan et al., 2007; Webber and Zbilut, 2005). In their original definition, RPs are symmetric $N \times N$ binary arrays (Marwan et al., 2007):

$$\mathbf{R}_{n,m}(\varepsilon) = \Theta(\varepsilon - \|\mathbf{X}_n - \mathbf{X}_m\|), \tag{2}$$

where $\boldsymbol{X}_n$ is the trajectory at time n, ε is a threshold (which has to be chosen carefully (Marwan et al., 2007)), $\Theta(\cdot)$ is the Heavyside function, and $\|\cdot\|$ is a norm. In case of a time-series with M regions, $\boldsymbol{X}_n$ would have dimensions $Mx1$. Usually, the trajectory is reconstructed from a time-

series **x** by means of time delayed embedding (Marwan et al., 2007). However, here we use the Spearman correlation between the IAC FC time-series instead of the norm in Eq. 2, in order to avoid choosing an arbitrary threshold, so that the RP becomes (Tewarie et al., 2019):

$$\mathbf{R}_{n,m} = \mathrm{corr}[IAC(n), IAC(m)]. \quad (3)$$

By doing this, we get an RP that displays how the functional network returns to similar configurations.

The IAC FC-based RPs can be used to show the points in time where the system transitions to other states by computing the gradients along the diagonal and setting the local maxima in the gradient matrix; this information reveals transitions to other states, as boundary points for data-driven windows (Tewarie et al., 2019). These data-driven windows identify periods in which the FC is similar across the brain, and have the added advantage of mitigating the effects of noisy estimates of instantaneous FC. The only constraint set was that the minimum distance between local maxima was of at least one oscillation of the frequency band of interest (Tewarie et al., 2019). Supplementary figure S1 shows a schematic overview of the approach. After setting the data-driven windows, the IAC was temporally averaged over these windows; thus, a temporally aggregated RP was computed with the windowed IAC in order to reduce noise and make the next analysis step computationally feasible.

3.2.3. Meta-state extraction by means of community detection

Community detection has been used in FC matrices themselves to uncover brain regions that are highly clustered and weakly connected to other regions (Bassett and Bullmore, 2006; Gates et al., 2016). However, in the present study we use a community detection algorithm to find which of the windowed FC matrices are highly correlated to others, similarly to Zhou et al. (2019). That is, we aim to find clusters of whole brain activity that repeat over time, identified as meta-states, in an unsupervised fashion. This eliminates one of the main disadvantages of most clustering methods, as well as other techniques for functional network detection such as hidden Markov models and non-negative tensor factorization, which is the fact that one has to *a priori* determine the number of communities to extract (Cabral et al., 2017; O'Neill et al., 2018; Ponce-Alvarez et al., 2015; Tewarie et al., 2019).

When viewing the RP as a graph, each data-driven window is a node, and the Spearman correlation between windows are the edges between the nodes. Thus, the RP can be seen as a weighted graph (since edges can be any value from -1 to 1) differentiating stronger and weaker correlations (Zhou et al., 2019). In order to detect repeating communities (meta-states) in the RP, we used the Louvain GJA method, a hierarchical clustering approach that maximizes the modularity score (Gates et al., 2016). The modularity measures the strength of links within a community compared to links outside the said community (Gates et al., 2016). The Louvain GJA method (Rubinov and Sporns, 2011) is an improved version of the algorithm originally described by (Blondel et al. (2008)). It initializes each node in its own community and then identifies the local maxima of the modularity score by looking at its changes iteratively when moving nodes to other communities (Gates et al., 2016). It has been proven to be robust in the presence of poorly defined communities (i.e., communities with medium to high correlations between them and unequally sized communities (Gates et al., 2016)). Since the algorithm is non-deterministic, we ran it 100 times and kept the solution with the highest modularity (Gates et al., 2016). We used the implementation of the Louvain GJA algorithm from the brain connectivity toolbox Rubinov and Sporns (2010).

As indicated in Fig. 1, two types of community analyses were performed:

- **Per-subject community detection:** a RP based on the windowed IAC was computed for each subject and community detection was performed on each individually. Then, the spatial patterns of each community (meta-state) for each individual subject were obtained by averaging the windowed IAC FC matrices that belonged to the same meta-state.
- **Per-group community detection:** the same procedure as in per-subject community detection, except that the RPs were constructed from the concatenated windowed IAC of *all* subjects in each group.

3.2.4. Meta-state temporal activation sequence (TAS) and instantaneous correlation tensor (ICT)

Once the meta-states were obtained from the windowed IAC FC matrices, to further dive into the temporal fluctuations, each of the temporal samples in the original, non-windowed FC time series was assigned to the closest meta-state by means of the Spearman correlation distance. The resulting symbolic time series, which we named *temporal activation sequence* (TAS), shows the temporal evolution of the dominant meta-states during the 60-s EEG recording. The concept of the TAS as discrete state time courses has been previously applied to characterize transitions between brain states (e.g., in the context of hidden Markov models applied to MEG (Baker et al., 2014) and fMRI leading eigenvector decomposition (Cabral et al., 2017)). Moreover, the characterization of discrete dynamic network switching by means of *Leading Eigenvector Dynamic Analysis* has recently been mathematically formalized and validated with a large dataset (Vohryzek et al., 2020). The instantaneous correlation tensors (ICT) can also be used to compute parameters of brain activation and serve as a representation of continuous activation of brain states, complementing the discrete representation of the TAS. Fig. 2 displays a sample TAS, as well as the associated ICT. Two types of metrics were computed in the next step: measures derived in terms of the discrete states (TAS) (Fig. 2, upper panel), and measures based on the continuous correlation (ICT) (Fig. 2, lower panel). Supplementary material video SV1 shows a visual representation of the TAS and ICT in real time for a cognitively healthy subject and an AD patient.

3.2.5. Metrics of meta-state activation

Along with the modularity, two parameters were extracted from the TAS (average dwell time and TAS complexity), one from the continuous correlations (instantaneous correlation speed) and one from information from both the TAS and the continuous correlation (leap size). These parameters provide information about the underlying temporal structure of the brain networks, the flexibility and variability of brain activation during rest, and the biological cost of meta-state switching:

Average dwell time. This parameter (also referred to in the literature as "life time" (Baker et al., 2014) measures the time the brain spends in the same dominant meta-state on average, and has been widely used in studies of dynamic brain state switching (Baker et al., 2014; Cabral et al., 2017; Schumacher et al., 2019; Vohryzek et al., 2020).

TAS complexity. In order to efficiently capture the underlying structural richness of temporal meta-state sequencing, we used the Lempel-Ziv complexity (LZC). The LZC is a non-parametric measure of complexity for one-dimensional signals that relates to the amount of distinct substrings and their rate of occurrence (Abásolo et al., 2006). A higher LZC indicates that the data is more complex (Abásolo et al., 2006). The LZC algorithm is described in (Abásolo et al., 2006), with the only difference here being that the TAS is already a finite symbol sequence, thus no conversion is needed.

Instantaneous correlation speed (ICS). The ICT is a measure of the Spearman correlation of each meta-state at each time point (dimensions $K \times T$, where K is the number of meta-states and T is the number of temporal samples in the 60-s EEG segment), and can thus be seen as a temporally changing position vector, where each spatial coordinate corresponds to a meta-state. The ICT can therefore be seen as a representation of how the meta-states dynamically attract the resting brain towards a specific network configuration.

Considering the difference in meta-state correlation position between consecutive time points as a displacement vector $\vec{r}$, the instantaneous correlation velocity can be easily calculated as its derivative with

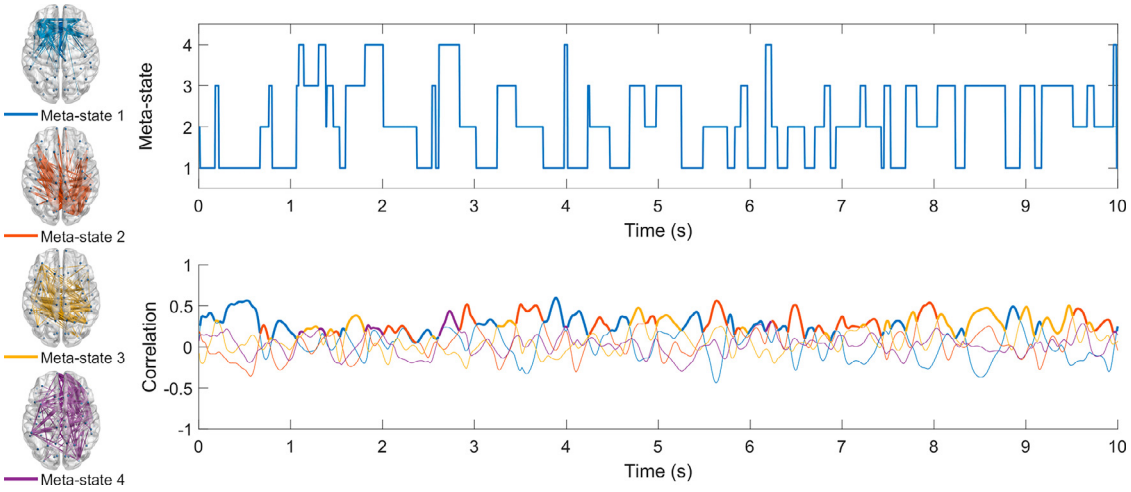

Fig. 2. Temporal activation sequence (upper diagram) and instantaneous correlation tensor (lower diagram) for a sample patient with AD for the first 10 seconds of the recording in the alpha band. The temporal activation sequence is a symbolic representation that shows the dominant meta-states at each time point. The highest correlation at each time point is marked with a bold line. Brain plots for each meta-state are also represented. As can be observed, more than one state can be correlated with the instantaneous FC at one time point.

respect to time $\vec{v} = \vec{r'}$. The ICS is the magnitude of the instantaneous correlation velocity $s = |\vec{v}|$. Fig. 2 and supplementary material video SV1 show a visual representation of the temporal evolution of meta-state correlations (SV1 shows a real-time representation in polar coordinates). In order to characterize the dynamic flexibility of the brain during meta-state switching, we computed both the mean and the standard deviation of the ICS.

Leap size. The leap size is a measure that characterizes the metabolic cost of transitioning from one meta-state to another; it is computed as the distance between one meta-state and the next (Ramirez-Mahaluf et al., 2020). We calculated the leap size as 1 - the Spearman correlation coefficient of the consecutive IAC FC matrices when a meta-state transition occurred (Ramirez-Mahaluf et al., 2020). Thus, this measure is derived from both the ICT and the TAS.

Modularity. The modularity is a measure of the strength of links within a community compared to links outside the community (Gates et al., 2016). In other words, it can be seen as an indicator of how well the communities within the graph are partitioned, with higher values meaning more clustered communities (Gates et al., 2016). In this case, we interpreted this measure as indicating how well defined and separated the meta-states for each subject were. The modulation values used here were those obtained from the Louvain GJA algorithm during the per-subject community detection step.

3.2.6. Surrogate data for measure normalization

In order to evaluate whether the extracted measures of dynamic state behavior reflected real dFC and were not due to random fluctuations, we performed surrogate data testing (Hindriks et al., 2016). We constructed surrogate versions of each EEG recording by means of the amplitude adjusted Fourier transform (AAFT). It is an improvement of the phase randomization method of surrogate data construction (Prichard and Theiler, 1994) that retains the amplitude distribution of the original time series (Khambhati et al., 2018; Theiler et al., 1992). Crucially, we used the same sequence of random numbers for every ROI (uniform phase randomization) to ensure that the linear correlations were kept intact (in other words, to preserve static FC) (Hindriks et al., 2016; Khambhati et al., 2018).

As in Núñez et al. (2019b), all the measures were normalized by dividing them by the average values computed from 100 surrogate time series. Thus, values that cannot be explained by genuine fluctuations are closer to 1, while values that are far from 1 (higher or lower) reflect behavior that is intrinsically due to dFC. Moreover, this correction ensures that all the measures can be compared between groups (Núñez et al., 2019b).

3.3. Statistical analyses

An exploratory analysis was initially performed to assess the distribution of the average dwell time, TAS complexity, ICS, leap size and modularity. Normality was assessed with the Lilliefors test, while homoscedasticity was assessed with the Levene test. The results showed that the values did not meet parametric test conditions for all measures. Therefore, between-group differences were assessed with non-parametric tests.

We conducted exploratory Kruskal-Wallis tests on the dwell time, TAS complexity, ICS, leap size, and modularity values in all frequency bands under study to detect global interactions between the three groups. Afterwards, post-hoc Mann-Whitney *U*-tests were performed to assess pairwise between-group differences in the frequency bands that displayed global interactions. A false discovery rate (FDR) correction was used to control for type I error (Benjamini and Hochberg, 1995). FDR correction was applied to control for the number of bands (global interactions) and groups (pairwise comparisons), with a significance level of $\alpha = 0.05$. Signal processing and statistical analyses were performed using MATLAB® (version R2018a Mathworks, Natick, MA). The brain networks were visualized with the BrainNet Viewer (http://www.nitrc.org/projects/bnv/) (Xia et al. (2013)).

4. Results

4.1. Community detection

We first performed per-subject community detection to extract personalized meta-states in order to enable the computation of accurate TAS and ICT for each subject. Fig. 3 shows histograms with the number of communities that were found for the subjects in all groups and frequency bands. No statistically significant differences between groups for the distributions of the number of meta-states were found in any band ($p > .05$, Chi-squared test). It can be observed that the number of detected meta-states detected varied between 2 and 5. In the delta and theta bands, most subjects showed 4 meta-state network configurations, while in alpha, beta-1, and beta-2 the majority of subjects displayed 3 meta-states

Subsequently, per-group community detection was also performed to find generalized brain networks that encompassed the meta-states of

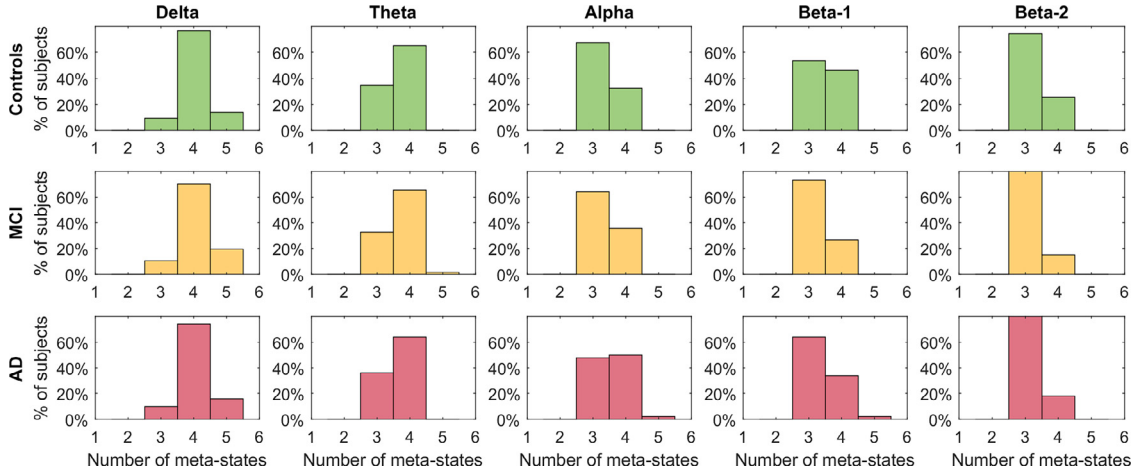

Fig. 3. Histograms depicting the number of communities (meta-states) detected by the Louvain GJA algorithm for all subjects and frequency bands.

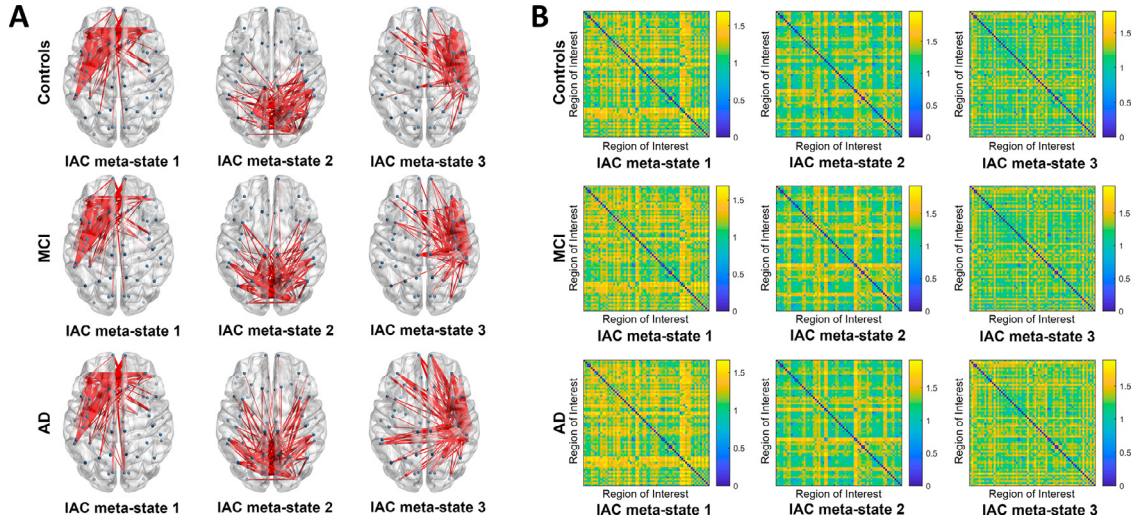

Fig. 4. Group meta-states for controls, patients with MCI, and patients with AD in the alpha band. Panel A shows brain plots with the 5% strongest connections of the meta-states obtained from performing community detection by means of the Louvain GJA method in RPs built from the data-driven windows of all subjects in a group (per-group community detection). Panel B displays the same meta-states as a matrix representation, where each axis represents the ROIs in the Desikan-Killiany atlas.

all subjects in a group. The meta-states found for each group in the alpha band are shown in Fig. 4 (the correspondence with specific ROIs in the Desikan-Killiany atlas for each row/column is displayed in figure S2 of the supplementary material). Spearman correlations between meta-states were also performed to assess spatial similarity, and are included in tables ST1 to ST3 of the supplementary material. We only display here the alpha-band meta-states, since it was the band where between-group differences were found for TAS-based measures (see the following section). The meta-states for the remaining bands (with the exception of beta-2, since community detection proved to be computationally unfeasible due to the large size of the whole-group RPs in this band) are shown in supplementary material figures S3 to S5. The meta-states are ordered according to the total number of appearances across time for all the subjects in the group. The results in the alpha band show three main meta-states for all groups: a frontal network with left-parietal connections (IAC meta-state 1), a predominantly parietal network with frontal connections (IAC meta-state 2), and a right-temporal network with some left-temporal, parietal and occipital connections (IAC meta-state 3).

4.2. Between-group comparisons for meta-state activation metrics

Fig. 5 displays the normalized average dwell time, TAS complexity, average and standard deviation of the ICS, average leap size, and average modularity values for all frequency bands. Statistically significant differences were mostly found in the alpha band for most of the measures.

Average dwell time. Statistically significant between group differences were found in the alpha band ($p = .041$, Kruskal-Wallis test, FDR corrected p-values). The control group displayed the longest dwell times of all three groups, with the post-hoc analysis showing that they were longer on average than for the ones for patients with MCI ($p = .055$, Mann-Whitney U-test, FDR corrected p-values) and dementia due to AD ($p = .007$, Mann-Whitney U-test, FDR corrected p-values). The controls were also the group with the highest proportion of subjects having longer average dwell times than those obtained with surrogate data.

TAS complexity. In the theta, alpha, beta-1, and beta-2 bands, most subjects displayed lower TAS complexity values than obtained for the surrogate data. This is the expected result, since it indicates a lower number of possible symbolic strings, in line with the concept of the system returning (and staying for a while) in previous states, as opposed to a surrogate with similar meta-states (sFC is not destroyed by AAFT, so the spatial patterns of meta-states are similar to the ones in the original time series), but no underlying dynamic structure. Statistically significant between group differences were found in the alpha band ($p = .026$, Kruskal-Wallis test, FDR corrected p-values). The post-hoc analysis revealed that controls had a less complex TAS sequence compared to both patients

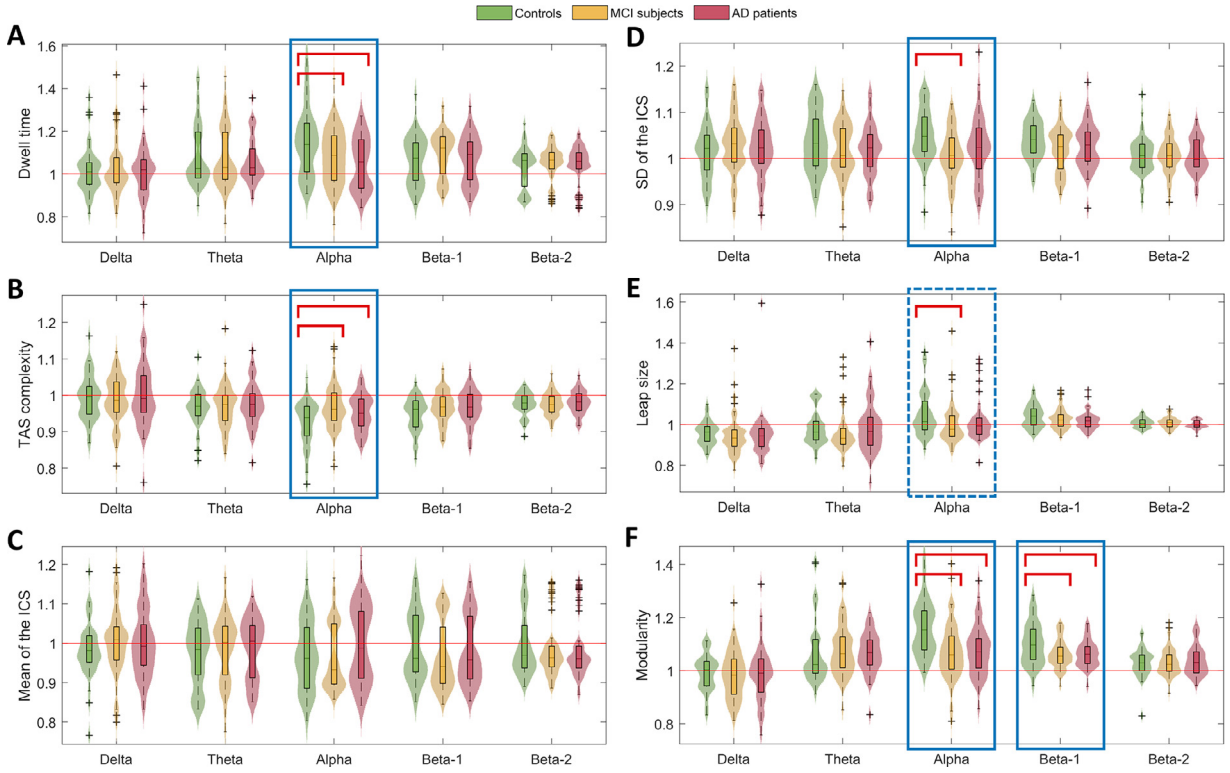

Fig. 5. Distribution plots depicting normalized (A) average dwell time, (B) TAS complexity, (C) average ICS, (D) standard deviation of the ICS, (E) average leap size, and (F) average modularity. The values were normalized by dividing the raw values by the average values extracted from 100 amplitude-adjusted Fourier transform (AAFT) surrogate versions of the original data. Values above the red line correspond to greater observed values for the original time series than for the surrogates (and vice-versa). Statistically significant between-group differences are marked with blue rectangles ($p < .05$, Kruskal-Wallis test, FDR corrected p-values), while differences that were significant before FDR correction ($p < .05$, Kruskal-Wallis test) are marked with dashed blue rectangles. Statistically significant post-hoc pairwise differences are marked with red brackets ($p < .05$, Mann-Whitney U-test, FDR corrected p-values). (For interpretation of the references to colour in this figure legend, the reader is referred to the web version of this article.)

with MCI ($p = .007$, Mann-Whitney U-test, FDR corrected p-values) and dementia due to AD ($p = .043$, Mann-Whitney U-test, FDR corrected p-values). Interestingly, patients with MCI showed values closer to the surrogates than patients with dementia due AD.

Mean and standard deviation of the ICS. The mean ICS showed no statistically significant differences between groups in any band ($p > .05$, Kruskal-Wallis test, FDR corrected p-values). Furthermore, around half of the subjects displayed values that were similar to those for the surrogates, indicating that the mean ICS is not affected by the dynamic behavior of resting-state EEG activity. In contrast, the standard deviation of the ICS was, for most of the subjects, higher than expected of surrogate data, meaning dFC has an effect on speed variability. The alpha band showed statistically significant group differences ($p = .006$, Kruskal-Wallis test, FDR corrected p-values), but only the MCI group displayed a statistically significant lower variability of the ICS than the control group ($p < .001$, Mann-Whitney U-test, FDR corrected p-values).

Average leap size. No statistically significant differences were found in any band, although the alpha band lost its statistical significance after FDR correction ($p = .1$, Kruskal-Wallis test, FDR corrected p-values), with controls showing a higher meta-state transition cost than patients with MCI ($p = .022$, Mann-Whitney U-test, FDR corrected p-values).

Average modularity. Statistically significant differences were found in the alpha ($p < .001$, Kruskal-Wallis test) and beta-1 bands ($p = .055$, Kruskal-Wallis test). Furthermore, controls showed higher modularity values than patients with MCI (alpha: $p = .03$, beta: $p = .03$, Mann-Whitney U-test, FDR corrected p-values), and patients with dementia due to AD in both bands (alpha: $p < .001$, beta-1: $p < .001$, Mann-Whitney U-test, FDR corrected p-values) indicating that the meta-states were more separated and better defined for the controls.

In order to test whether the mismatch in education level could have an effect on between-group comparisons, we tested for statistical differences in grand-average mean dwell time, TAS complexity, mean and standard deviation of the ICS, leap size and modularity between subjects with education level A and B for all groups (Mann-Whitney U-test). No statistical differences for any of the measures in any group or band were found ($p > .05$).

5. Discussion

We adopted a novel approach to investigate the dynamic formation of specific brain networks during rest by capturing aspects based on both the discrete activation of brain meta-states and the continuous description of the evolution of the meta-state strength. Our findings show that: (i) the proposed methodology is able to find meaningful meta-states in resting-state EEG recordings (ii) MCI and AD do not affect the spatial profile of the main meta-states that appear during rest, but they are less well defined; (iii) MCI and AD meta-states are briefer and less dynamically structured than those of cognitively healthy elderly controls; and (iv) healthy controls display a higher dynamic flexibility than patients with MCI, as their brain networks are more dynamically pulled towards meta-states (attractors).

5.1. Detection and characterization of group meta-states

Our first objective was to identify dynamic functional meta-states in the EEG activity of the population under study. When conducting a whole-group analysis in the alpha band, 3 meta-states were found for all groups. One must exercise caution when identifying these meta-states as specific resting-state networks, since the more well-known ones are

usually based on blood-oxygen-level dependent imaging (BOLD), not on EEG (Damoiseaux et al., 2006). For all three groups (controls, MCI, and AD), the number of communities converged to 3 as the frequency increased. The number of available data-driven windows increases with frequency, and graph community detection algorithms usually behave better with larger graphs (Gates et al., 2016). Thus, we hypothesized that the number of dominant group meta-states with Louvain GJA as the community detection algorithm in the 60-s EEG recordings is closer to 3. In order to test this, we performed an additional test on the 16 control subjects who had two minutes of artifact-free EEG recordings available. We performed the same community detection as in the main study but changed the length of the analyzed data-segment from 1 to 120 s in steps of 1 s. The results (supplementary material figure S6) show a clear convergence to 3 communities in the theta, alpha, beta-1, and beta-2 bands. We did not perform this analysis in the delta band due to the data segment not being long enough to define data-driven windows for very short epochs.

Our results suggest that MCI and AD do not directly affect the "global" EEG spatial patterns of resting-state networks themselves. However, the alpha and beta-1 modularity decrease found in MCI and AD suggests that their EEG resting-state networks are more diffuse and less well defined, i.e., the networks that dynamically form and dissolve are not as well differentiated in MCI and AD compared to healthy elderly controls. Interestingly, average sFC IAC values were lower in controls compared to patients with MCI and dementia due to AD in the alpha band (see supplementary material figure S7). This result could imply that MCI and AD induce global alpha hyperconnectivity that is associated with loss of network definition. It is worth noting that disparate results can be found in the literature when it comes to sFC in MCI and AD: while some studies have also found hyperconnectivity between specific brain regions in patients with AD (Fu et al., 2019) and in early stages of dementia (Bonanni et al., 2020), the opposite behavior has been reported as well (Babiloni et al., 2016b; Briels et al., 2020). Nonetheless, it is worth mentioning that when computing AEC based on a sliding window approach (with window sizes of 0.5, 15 and 60 s, see supplementary material figure S8) we found that the results showed a decrease in sFC in the alpha band for patients with AD for sliding window sizes of 15 and 60 s. This disagreement could be due to a variety of reasons, such as the fact that IAC is more suitable for the characterization of fast connectivity than AEC Tewarie et al. (2019). It could also be the case that AD induces an increase in very fast bursts of instantaneous connectivity that are canceled when averaging across long windows. This is supported by the fact that simulations have shown that AEC correlation with ground truth states was maximal for window lengths that matched state duration Liuzzi et al. (2019). We also calculated the Spearman correlation between the average IAC and the relative power of each band and found that they were weak and not statistically significant (see supplementary material figure S9). Moreover, there were statistically significant differences in relative power between groups in the theta and beta-1 bands, with patients with AD showing clear power shifts towards lower frequencies and patients with MCI also displaying these shifts to a lesser degree (see supplementary material figure S10). Crucially, there were no statistically significant differences in alpha relative power, which supports the notion that instantaneous FC is less affected by relative power than traditional windowed FC. Additionally, scalp topographies of the relative power of each group meta-state in the alpha band were obtained (see supplementary material figure S11) and no statistically significant differences in relative power between meta-states was found, indicating that network activation patterns appear to be independent from raw power.

We also obtained scalp topographies of the meta-states in the alpha band in order to compare with traditional EEG microstates and assess possible relationships between them and network meta-sates (Khanna et al., 2015). The scalp topographies were obtained by averaging the EEG time-series from the 19 scalp recordings in each of the data-driven windows. Then, the windowed EEG was averaged again for all the data-driven windows corresponding to each specific meta-state (see supplementary material figure S12). The scalp topographies corresponding to each meta-state were different for each group, and for the most part did not resemble the four traditional EEG microstate topologies. Possible exceptions are control meta-state 1, which resembles microstate D, AD meta-state 1 and MCI meta-state 3, which resemble microstate C, and AD meta-states 2 and 3, which resemble microstate B (Khanna et al., 2015). This suggests that source-level network meta-states are independent from scalp activation to some extent.

Our results do not necessarily mean that the brain only passes through 3 meta-states during rest, but that these 3 topologies were the predominant ones on the EEG time scale. Interestingly, an fMRI-based study that performed community detection with a similar method also found 3 states in healthy young subjects (Zhou et al., 2019). Another fMRI study obtained an optimal number of 3 communities using *k*-means clustering to detect functional states in patients with AD and dementia with Lewy bodies (Schumacher et al., 2019). Other fMRI studies that have tried to identify meta-states found different numbers of FC states. For example, Cabral *et al.* found 5 FC states in healthy controls during rest with their *Leading Eigenvector Dynamic Analysis* methodology (Cabral et al., 2017), while Fu *et al.* found 4 states in controls, patients with AD, and patients with subcortical ischemic vascular disease using *k*-means clustering (Fu et al., 2019). We hypothesize that the 3 meta-states characterized by our methodology are a dominant subset from the full repertoire that could be detectable with other techniques, like the ones previously mentioned or Hidden Markov Models (see Baker et al. (2014); Hunyadi et al. (2019); Vidaurre et al. (2018)). Furthermore, the results do not necessarily imply that all subjects displayed the same individual meta-states. When taken together, the individual network configurations aggregate into 3 meta-states that can be seen as a "summary" of the underlying networks. However, one must take into account that these meta-states were computed as the average of a large number of windows that belong to different subjects. Thus, individual idiosyncrasies or subtle differences are lost in these group meta-states (Hutchison et al., 2013). Some subject-specific states also get lost when performing whole-group community detection (Gu et al., 2020; Schumacher et al., 2019), which explains the apparent discrepancy between the number of whole-group meta-states and some subjects who showed 4 individual meta-states.

It was also observed that, while the ongoing resting-state EEG always has a dominant meta-state, the ICT shows that the instantaneous FC is often correlated with more than one network configuration. This leads us to believe that meta-states are not mutually exclusive and are more a representation of individual, well-defined network configurations that can be simultaneously active. This is in line with non-negative tensor factorization analyses, in which all the states are active at all times, only with different strengths (Ponce-Alvarez et al., 2015; Tewarie et al., 2019). These transient states emerge and dissolve in a non-discrete fashion, just as they do in the present study. Thus, our results support the notion of the brain being a metastable system in which the meta-states act as attractors which pull the functional network with variable strength, but never settle for long into a specific one (Tognoli and Kelso, 2014; Vohryzek et al., 2020).

5.2. MCI- And AD-induced alterations to dynamic meta-state switching

The second objective of the study was to explore how MCI and AD might influence normal meta-state sequences during rest. The results for the average dwell time, TAS complexity, and standard deviation of the ICS in the alpha band confirm our hypothesis that these diseases may induce a loss in dynamic state fluctuations and break the underlying structure of the state sequences.

We already found evidence of the presence of dFC in cognitively healthy elderly controls, patients with MCI, and patients with dementia due to AD in a previous work, in which dFC was measured by means of sliding windows and the amplitude envelope correlation (AEC)

(Núñez et al., 2019b). The present study further strengthens those findings. The less due to dFC the observed measures of meta-state shifting are, the closer the values of each extracted measure will be to 1. Thus, it is clear from the results that brain meta-state shifting in patients with MCI and AD is more unstable and less structured, and more influenced by sFC and other factors than in the controls. The importance of conducting surrogate testing when assessing the presence of dFC-related metrics cannot be understated. If one does not normalize, the results can be misleading and reflect differences that can be due to random fluctuations in static FC (Hindriks et al., 2016). To test this, we conducted two additional tests: first, we performed the same between-group comparisons for the surrogate data alone (see supplementary material figure S13), and we found statistically significant differences in the theta and beta-1 bands, but not in alpha. The between-group differences could be due to differences in power, static FC, or even noisier segments for patients with AD. However, the values in alpha for most measures show statistically significant differences after normalizing by means of the surrogate data. This indicates that these differences should be almost entirely due to dFC. Secondly, we compared the original, non-normalized values of all the measures for the three groups separately with the average of their corresponding surrogate data (see supplementary material figures S14 to S16). For the control group there were statistically significant differences between the measures derived from the original time-series and the ones derived from the surrogates in alpha for all measures except the mean of the ICS (which did not show statistically significant differences between groups after normalization either). This further supports the notion that the differences in the alpha band are due to differences in dFC between groups, and, in some cases, due to the lack of alpha dFC in the MCI and AD groups.

We observed that average dwell times were significantly lower for patients with MCI and AD compared with controls. Previous research has already shown AD patients spending less time in default mode network states (Jones et al., 2012). Some fMRI studies found evidence of patients with AD having shorter dwell times in baseline states and longer times in weaker states (Fu et al., 2019; Gu et al., 2020). Our study does not distinguish between these two types of states (weakly and strongly connected), but our findings point to EEG meta-states being more transient in MCI and AD. We speculate that this could be related to how meta-states are less defined in these groups, which could lead to them "dominating" over others for shorter times. If the assumption is made that each meta-state corresponds to a specific active module focused on a functional quality (Jones et al., 2012), then this might mean that the MCI and AD brain is associated with more unstable cognition. However, alternative explanations must be considered as well; it may be possible that more transient meta-states could be a sign of more flexible cognition in patients with MCI and AD, perhaps as a compensatory mechanism, although such behavior has usually only been suggested in patients with MCI and preclinical or early AD (Gaubert et al., 2019; Jones et al., 2016; Maestú et al., 2011).

We hypothesize that the TAS complexity results are evidence of the existence of an underlying structure in the sequence of meta-states in healthy controls. Controls show a relatively limited amount of possible meta-state sequences when compared to the pathological groups. This finding suggests that meta-state sequencing is not entirely arbitrary. The fact that meta-state transitions are not completely random has been previously suggested (Vidaurre et al., 2017). Thus, it can be inferred that MCI and AD induce changes into these meta-state transition sequences leading to a loss of some of their structure and an increase of their randomness. It has been observed that staying in the same meta-state for consecutive windows could be a way to keep transition networks cost-efficient (Ramirez-Mahaluf et al., 2020; Zalesky et al., 2014). Furthermore, higher cognition has also been correlated with efficient planning of meta-state switching (Ramirez-Mahaluf et al., 2020). It is important to highlight that the TAS complexity measures the complexity of the symbolic activation sequence of the meta-state activation patterns, not the raw EEG data, since EEG complexity has been found to be reduced in AD when compared to controls (Abásolo et al., 2006). Although we observed that the control group showed a tendency towards higher metabolic cost when transitioning to another dominant meta-state, they stayed in the same dominant state for longer times. This could indicate that controls make fewer, but more substantial meta-state transitions than patients with MCI or dementia due to AD.

Our results showed that the mean ICS is not a property intrinsically due to dFC and thus cannot be associated with any MCI- or AD-induced alterations in dynamic network switching. However, the higher standard deviation of the ICS in controls compared to MCI points to a deficit of alpha dynamic brain flexibility that is at least partially recovered in subjects that have progressed to AD. In a previous study (conducted at scalp-level), we found an overall decrease in alpha non-stationarity in patients with MCI that was more pronounced than in patients with AD (Núñez et al., 2020). We speculate that the reduced dynamic flexibility may be related to the more stationary sensor-level EEG activity, which could be linked to the hypothesis that MCI displays excessive neuronal activity possibly leading to amyloid deposition (de Haan et al., 2012). In this case, excessive, stationary activity would lead to steadier and less fluctuating movement between network configurations, with less sudden changes in attraction towards specific meta-states.

In order to assess the reliability of the methodology, we repeated the whole procedure on the second minute of resting-state activity and the full 120-s segments, on the subjects that had two minutes of artifact-free EEG data available (16 controls, 29 patients with MCI and 27 patients with AD). The main results are displayed in supplementary material figures S17 and S19 (group meta-states in the alpha band for the second minute of activity and the full 120-s segment respectively), as well as S18 and S20 (between-group comparisons for the normalized measures, for the second minute of activity and the full 120-s segment respectively). The group meta-states closely resemble the ones found for the full database, with small differences in network topology most likely due to the small number of subjects (especially for the control group). No statistically significant differences were found, most likely due to the reduced number of subjects when compared to the full database. The overall tendencies for all measures, however, were the same as in the main results.

Several studies have tried to characterize the mechanisms of dynamic integration of information that occur at the system-level by means of computational modeling Cabral et al. (2014); Deco et al. (2017a, 2013). These resting-state models share the common trait that structured fluctuations emerge when the system is at a point of bifurcation, or point of criticality, between steady state and oscillatory regime where multistable states appear Cabral et al. (2014); Deco et al. (2017a, 2013). This remarkably fits with our findings of attractors that dynamically pull the system into meta-states. Moreover, it has also been shown that oscillator-based models modulate frequency-specific amplitude fluctuations and show good fit with empirical MEG data Cabral et al. (2014); Deco et al. (2017a). In this respect, our findings are in line with the behavior reported in these studies, since the alterations in dynamic alpha IAC patterns could be linked to impairment of meta-stable formation of large-scale networks in MCI and AD. These would lead to diminished correlated amplitude fluctuations in this frequency band Cabral et al. (2014); Deco et al. (2017a).

5.3. Limitations and future research lines

This study has several limitations that merit further attention. Firstly, we tried to solve the well-known problem of having to choose a window size to measure dFC by means of sliding windows by using a measure of instantaneous FC (i.e., IAC). However, these measures come with the hurdle of lower SNR, as well as higher memory requirements for computational processing of the connectivity matrices. We used data-driven windows based on RPs to address both issues. However, alternative methods to build data-driven windows could be explored in future works, such as single-scale time-dependent windows (Zhuang et al.,

2020). It is also worth mentioning that the IAC is not sensitive to oscillation power, and Hidden Markov Model-based studies have found states that are characterized by increased or decreased oscillation power Baker et al. (2014). Thus, it could be the case that due to the limitations of IAC some meta-states could be obfuscated.

The method proposed in this study is not without its limitations. Even though the between-group comparisons survive FDR statistical correction, this does not mean that improvements could not be made to the processing pipeline. In particular, it is possible that our method lacks sensitivity which could lead to the detection of fewer states than the ones that are present. We used the Louvain GJA algorithm to detect communities in the RPs due to its advantages, although this algorithm has some limitations (both are indicated in Section 3.2.3) (Gates et al., 2016). It would be interesting to analyze whether other community detection algorithms, such as Walktrap, Newman's Spectral Approach, Infomap, Label Propagation or non-backtracking matrix (Gates et al., 2016; Krzakala et al., 2013), lead to similar results. It is possible, however, that other community detection methods could lead to an increased number of false positives. Of note, we characterized how the recording length affected the number of communities that the Louvain GJA detected (see Supplementary Material figure S6). We found that it converged to three in the theta, alpha, beta-1, and beta-2 bands. Thus, observing how the communities detected vary according to each algorithm could be an interesting study in itself, since it could be possible that some algorithms could identify more meta-states or have more reproducible results.

While it is not possible to characterize the specific properties, such as average dwell time, inter-state intervals or fractional occupancy of the "group" meta-states, due to the fact that they are not specifically associated to specific "per-subject" meta-states, it has been reported that some MEG states, such as those in the bilateral default and dorsal attention networks, have reduced duration in patients with AD compared to cognitively healthy controls (Sitnikova et al., 2018). It would be interesting to perform an analysis where meta-state characterization is done only at the group level. This would enable direct comparison between the specific state properties of each group, while losing the precision that per-subject meta-state characterization facilitates.

Due to the exploratory nature of the study, and the fact that the metrics of meta-state correlation were measuring relatively independent properties of the dynamic activation of meta-states, we only corrected the p-values for the number of bands. However, a stricter correction for the global interactions was also performed (correcting for the number of bands and the number of measures) and is included in the supplementary material (table ST4). With this strict correction, the average dwell time and the TAS complexity lose statistically significant differences in the alpha band ($p = .062$ and $p = .053$ respectively), and the modularity loses statistically significant differences in the beta-1 band ($p = .110$).

The influence of sFC was minimized by the use of surrogate normalization, but the fact that the behavioral variability found in patients with MCI and dementia due to AD could be underpinned by sFC and structural connectivity cannot be overlooked. It might be the case that the between-group differences explained by dFC could be, at least partially, indirectly caused by abnormal sFC and structural connectivity. Both of these have been previously observed in patients with MCI and dementia due to AD Pineda-Pardo et al. (2014), and account for the majority of the variance in fMRI data from individuals Vidaurre et al. (2019). Thus, it is important to point out that structural connectivity, sFC and dFC are complementary techniques, with dFC having been associated with behavioral traits not dominated by anatomy, but more complex cognitive functions Vidaurre et al. (2019).

Another interesting research line could be replicating the results with different databases, not only EEG-based but MEG ones as well. MEG signals are less sensitive to field spread and volume conduction (Lai et al., 2018). An important limitation of the study is the fact that the 68 ROI time-courses were estimated from 19 EEG channels. Due to the limited spatial resolution of the source estimation, we avoided over-interpretation of the results by refering to relatively broad areas (e.g., left-temporal) instead of specific ROIs of the Desikan-Killiany atlas. Nonetheless, it is noteworthy that the meta-states that we extracted closely resemble some of the meta-states found for an MEG database using non-negative tensor factorization (Tewarie et al., 2019).

Finally, since the patients with MCI can usually be separated into two subgroups (the ones that eventually developed AD and the ones that remain stable in MCI condition), when that information becomes available, it would be of interest to investigate whether the two subgroups are closer in meta-state behavior to the controls and the patients with AD, respectively. This could thereby identify early signs of neurodegeneration that are specific to AD in the MCI-AD continuum. To achieve this, it would also be interesting to expand the database so that all patient subgroups and the control group can be matched in number of subjects.

6. Conclusion

In the present study, we applied a novel methodology to detect meta-states and their temporal sequencing in resting-state EEG recordings from controls, as well as patients with MCI and dementia due to AD. Our approach revealed that MCI and AD do not change the network topology of the main meta-states, but they induce a loss of flexibility and definition of neural networks when the brain moves through meta-state space. These alterations are characterized by a decrease in modularity, shorter dominant meta-state dwell times, diminished metabolic cost of state transition, and decrease in variability of the correlation speed. All these results point to an overall more erratic dynamic behavior of the brain during rest, coupled with weaker meta-state differentiation, possibly associated with unstable cognition. Furthermore, we also showed that dynamic state switching is not entirely random, with an underlying transition sequence structure that is also partially lost as the MCI-AD continuum progresses. We believe this work could be a starting step towards a comprehensive characterization of the spatio-temporal dynamics of functional network switching in the MCI-AD continuum.

Credit authorship contribution statement

Pablo Núñez: Conceptualization, Methodology, Software, Formal analysis, Investigation, Writing - original draft, Visualization, Data curation. **Jesús Poza:** Conceptualization, Methodology, Data curation, Writing - review & editing, Visualization, Supervision, Funding acquisition. **Carlos Gómez:** Conceptualization, Methodology, Data curation, Writing - review & editing. **Víctor Rodríguez-González:** Formal analysis, Writing - review & editing. **Arjan Hillebrand:** Methodology, Writing - review & editing. **Prejaas Tewarie:** Methodology, Software, Writing - review & editing. **Miguel Ángel Tola-Arribas:** Resources, Data curation, Writing - review & editing. **Mónica Cano:** Data curation, Writing - review & editing. **Roberto Hornero:** Conceptualization, Writing - review & editing, Supervision.

Acknowledgements

This research was supported by 'Ministerio de Ciencia e Innovación - Agencia Estatal de Investigación' and 'European Regional Development Fund' (FEDER) and 'Ministerio de Ciencia, Innovación y Universidades' under projects PGC2018-098214-A-I00, the 'European Commission' and FEDER under project 'Análisis y correlación entre el genoma completo y la actividad cerebral para la ayuda en el diagnóstico de la enfermedad de Alzheimer' and 'Análisis y correlación entre la epigenética y la actividad cerebral para evaluar el riesgo de migraña crónica y episódica en mujeres' ('Cooperation Programme Interreg V-A Spain-Portugal POCTEP 2014–2020'), and by CIBER-BBN (ISCIII) co-funded with FEDER funds. P. Núñez was in receipt of a predoctoral scholarship 'Ayuda para contratos predoctorales para la Formación de Profesorado Universitario (FPU)' grant from the 'Ministerio de Educación, Cultura

y Deporte' (FPU17/00850). V. Rodríguez-González was in receipt of a PIF-UVa grant from the 'University of Valladolid'.

Supplementary material

Supplementary material associated with this article can be found, in the online version, at 10.1016/j.neuroimage.2021.117898

References

Abásolo, D., Hornero, R., Gómez, C., García, M., López, M., 2006. Analysis of EEG background activity in Alzheimer's disease patients with lempel-Ziv complexity and central tendency measure. Medical Engineering and Physics 28 (4), 315–322. doi:10.1016/j.medengphy.2005.07.004.

Albert, M.S., DeKosky, S.T., Dickson, D., Dubois, B., Feldman, H.H., Fox, N.C., Gamst, A., Holtzman, D.M., Jagust, W.J., Petersen, R.C., Snyder, P.J., Carrillo, M.C., Thies, B., Phelps, C.H., et al., 2011. The diagnosis of mild cognitive impairment due to Alzheimer's disease: recommendations from the national institute on aging-Alzheimer's association workgroups on diagnostic guidelines for Alzheimer's disease. Alzheimer's and Dementia 7 (3), 270–279. doi:10.1016/j.jalz.2011.03.008.

Babiloni, C., Del Percio, C., Caroli, A., Salvatore, E., Nicolai, E., Marzano, N., Lizio, R., Cavedo, E., Landau, S., Chen, K., Jagust, W., Reiman, E., Tedeschi, G., Montella, P., De Stefano, M., Gesualdo, L., Frisoni, G.B., Soricelli, A., 2016. Cortical sources of resting state EEG rhythms are related to brain hypometabolism in subjects with Alzheimer's disease: an EEG-PET study. Neurobiol. Aging 48, 122–134. doi:10.1016/j.neurobiolaging.2016.08.021. https://linkinghub.elsevier.com/retrieve/pii/S0197458016301993

Babiloni, C., Lizio, R., Marzano, N., Capotosto, P., Soricelli, A., Triggiani, A.I., Cordone, S., Gesualdo, L., Del Percio, C., et al., 2016. Brain neural synchronization and functional coupling in Alzheimer's disease as revealed by resting state EEG rhythms. International Journal of Psychophysiology 103, 88–102. doi:10.1016/j.ijpsycho.2015.02.008. https://linkinghub.elsevier.com/retrieve/pii/S0167876015000380

Baker, A.P., Brookes, M.J., Rezek, I.A., Smith, S.M., Behrens, T., Probert Smith, P.J., Woolrich, M., 2014. Fast transient networks in spontaneous human brain activity. Elife 3 (3), 1–18. doi:10.7554/eLife.01867.

Bassett, D.S., Bullmore, E., 2006. Small-world brain networks. Neuroscientist 12 (6), 512–523. doi:10.1177/1073858406293182.

Bassett, D.S., Porter, M.A., Wymbs, N.F., Grafton, S.T., Carlson, J.M., Mucha, P.J., 2013. Robust detection of dynamic community structure in networks. Chaos: An Interdisciplinary Journal of Nonlinear Science 23 (1), 013142. doi:10.1063/1.4790830. http://aip.scitation.org/doi/10.1063/1.4790830

Benjamini, Y., Hochberg, Y., 1995. Controlling the false discovery rate: a practical and powerful approach to multiple testing. Journal of the Royal Statistical Society 57 (1), 289–300. doi:10.2307/2346101.

Blondel, V.D., Guillaume, J.-L., Lambiotte, R., Lefebvre, E., 2008. Fast unfolding of communities in large networks. J. Stat. Mech: Theory Exp. 2008 (10), P10008. doi:10.1088/1742-5468/2008/10/P10008.

Bonanni, L., Moretti, D., Benussi, A., Ferri, L., Russo, M., Carrarini, C., Barbone, F., Arnaldi, D., Falasca, N.W., Koch, G., Cagnin, A., Nobili, F., Babiloni, C., Borroni, B., Padovani, A., Onofrj, M., Franciotti, R., 2020. Hyperconnectivity in dementia is early and focal and wanes with progression. Cerebral Cortex 1–9. doi:10.1093/cercor/bhaa209. https://academic.oup.com/cercor/advance-article/doi/10.1093/cercor/bhaa209/5892783

Briels, C.T., Schoonhoven, D.N., Stam, C.J., de Waal, H., Scheltens, P., Gouw, A.A., 2020. Reproducibility of EEG functional connectivity in Alzheimer's disease. Alzheimer's Research & Therapy 12 (1), 68. doi:10.1186/s13195-020-00632-3.

Brookes, M.J., Hale, J.R., Zumer, J.M., Stevenson, C.M., Francis, S.T., Barnes, G.R., Owen, J.P., Morris, P.G., Nagarajan, S.S., 2011. Measuring functional connectivity using MEG: methodology and comparison with fcMRI. Neuroimage 56 (3), 1082–1104. doi:10.1016/j.neuroimage.2011.02.054. https://linkinghub.elsevier.com/retrieve/pii/S1053811911002102

Brookes, M.J., O'Neill, G.C., Hall, E.L., Woolrich, M.W., Baker, A., Palazzo Corner, S., Robson, S.E., Morris, P.G., Barnes, G.R., et al., 2014. Measuring temporal, spectral and spatial changes in electrophysiological brain network connectivity. Neuroimage 91, 282–299. doi:10.1016/j.neuroimage.2013.12.066.

Cabral, J., Luckhoo, H., Woolrich, M., Joensson, M., Mohseni, H., Baker, A., Kringelbach, M.L., Deco, G., 2014. Exploring mechanisms of spontaneous functional connectivity in MEG: how delayed network interactions lead to structured amplitude envelopes of band-pass filtered oscillations. Neuroimage 90, 423–435. doi:10.1016/j.neuroimage.2013.11.047. https://linkinghub.elsevier.com/retrieve/pii/S1053811913011968

Cabral, J., Vidaurre, D., Marques, P., Magalhães, R., Silva Moreira, P., Miguel Soares, J., Deco, G., Sousa, N., Kringelbach, M.L., 2017. Cognitive performance in healthy older adults relates to spontaneous switching between states of functional connectivity during rest. Sci. Rep. 7 (1), 5135. doi:10.1038/s41598-017-05425-7.

Damoiseaux, J.S., Rombouts, S.A.R.B., Barkhof, F., Scheltens, P., Stam, C.J., Smith, S.M., Beckmann, C.F., 2006. Consistent resting-state networks across healthy subjects. Proceedings of the National Academy of Sciences 103 (37), 13848–13853. doi:10.1073/pnas.0601417103.

Deco, G., Cabral, J., Woolrich, M.W., Stevner, A.B.A., van Hartevelt, T.J., Kringelbach, M.L., 2017. Single or multiple frequency generators in on-going brain activity: a mechanistic whole-brain model of empirical MEG data. Neuroimage 152 (February), 538–550. doi:10.1016/j.neuroimage.2017.03.023. https://linkinghub.elsevier.com/retrieve/pii/S105381191730232X

Deco, G., Jirsa, V.K., McIntosh, A.R., 2013. Resting brains never rest: computational insights into potential cognitive architectures. Trends Neurosci. 36 (5), 268–274. doi:10.1016/j.tins.2013.03.001. https://linkinghub.elsevier.com/retrieve/pii/S0166223613000398

Deco, G., Kringelbach, M.L., Jirsa, V.K., Ritter, P., et al., 2017. The dynamics of resting fluctuations in the brain: metastability and its dynamical cortical core. Sci. Rep. 7 (1), 3095. doi:10.1038/s41598-017-03073-5.

Desikan, R.S., Ségonne, F., Fischl, B., Quinn, B.T., Dickerson, B.C., Blacker, D., Buckner, R.L., Dale, A.M., Maguire, R.P., Hyman, B.T., Albert, M.S., Killiany, R.J., 2006. An automated labeling system for subdividing the human cerebral cortex on MRI scans into gyral based regions of interest. Neuroimage 31 (3), 968–980. doi:10.1016/j.neuroimage.2006.01.021. https://linkinghub.elsevier.com/retrieve/pii/S1053811906000437

Douw, L., Nieboer, D., Stam, C.J., Tewarie, P., Hillebrand, A., 2018. Consistency of magnetoencephalographic functional connectivity and network reconstruction using a template versus native MRI for co-registration. Hum. Brain Mapp. 39 (1), 104–119. doi:10.1002/hbm.23827.

Fraschini, M., Demuru, M., Crobe, A., Marrosu, F., Stam, C.J., Hillebrand, A., et al., 2016. The effect of epoch length on estimated EEG functional connectivity and brain network organisation. J. Neural. Eng. 13 (3), 036015. doi:10.1088/1741-2560/13/3/036015. http://www.ncbi.nlm.nih.gov/pubmed/27137952

Fu, Z., Caprihan, A., Chen, J., Du, Y., Adair, J.C., Sui, J., Rosenberg, G.A., Calhoun, V.D., 2019. Altered static and dynamic functional network connectivity in Alzheimer's disease and subcortical ischemic vascular disease: shared and specific brain connectivity abnormalities. Hum. Brain Mapp. 40 (11), 3203–3221. doi:10.1002/hbm.24591.

Gates, K.M., Henry, T., Steinley, D., Fair, D.A., 2016. A monte carlo evaluation of weighted community detection algorithms. Front. Neuroinform. 10 (NOV), 1–16. doi:10.3389/fninf.2016.00045. http://journal.frontiersin.org/article/10.3389/fninf.2016.00045/full

Gaubert, S., Raimondo, F., Houot, M., Corsi, M.-C., Naccache, L., Diego Sitt, J., Hermann, B., Oudiette, D., Gagliardi, G., Habert, M.-O., Dubois, B., De Vico Fallani, F., Bakardjian, H., Epelbaum, S., Bakardjian, H., Benali, H., Bertin, H., Bonheur, J., Boukadida, L., Boukerrou, N., Cavedo, E., Chiesa, P., Colliot, O., Dubois, B., Dubois, M., Epelbaum, S., Gagliardi, G., Genthon, R., Habert, M.-O., Hampel, H., Houot, M., Kas, A., Lamari, F., Levy, M., Lista, S., Metzinger, C., Mochel, F., Nyasse, F., Poisson, C., Potier, M.-C., Revillon, M., Santos, A., Andrade, K.S., Sole, M., Surtee, M., de Schotten, M.T., Vergallo, A., Younsi, N., 2019. EEG Evidence of compensatory mechanisms in preclinical Alzheimer's disease. Brain 142 (6), 1497–1500. doi:10.1093/brain/awz150. https://academic.oup.com/brain/article/142/6/1497/5498977 https://academic.oup.com/brain/advance-article/doi/10.1093/brain/awz150/5519996

Gramfort, A., Papadopoulo, T., Olivi, E., Clerc, M., 2010. OpenMEEG: opensource software for quasistatic bioelectromagnetics. Biomed. Eng. Online 9 (1), 45. doi:10.1186/1475-925X-9-45. http://biomedical-engineering-online.biomedcentral.com/articles/10.1186/1475-925X-8-1

Gu, Y., Lin, Y., Huang, L., Ma, J., Zhang, J., Xiao, Y., Dai, Z., 2020. Abnormal dynamic functional connectivity in Alzheimer's disease. CNS Neuroscience and Therapeutics (April) 1–10. doi:10.1111/cns.13387.

de Haan, W., Mott, K., van Straaten, E.C.W., Scheltens, P., Stam, C.J., 2012. Activity dependent degeneration explains hub vulnerability in Alzheimer's disease. PLoS Comput. Biol. 8 (8), e1002582. doi:10.1371/journal.pcbi.1002582.

Hansen, E.C.A., Battaglia, D., Spiegler, A., Deco, G., Jirsa, V.K., et al., 2015. Functional connectivity dynamics: modeling the switching behavior of the resting state. Neuroimage 105, 525–535. doi:10.1016/j.neuroimage.2014.11.001.

Hindriks, R., Adhikari, M.H., Murayama, Y., Ganzetti, M., Mantini, D., Logothetis, N.K., Deco, G., et al., 2016. Can sliding-window correlations reveal dynamic functional connectivity in resting-state fMRI? Neuroimage 127, 242–256. doi:10.1016/j.neuroimage.2015.11.055.

Hunyadi, B., Woolrich, M.W., Quinn, A.J., Vidaurre, D., De Vos, M., 2019. A dynamic system of brain networks revealed by fast transient EEG fluctuations and their fMRI correlates. Neuroimage 185 (August 2018), 72–82. doi:10.1016/j.neuroimage.2018.09.082.

Hutchison, R.M., Womelsdorf, T., Allen, E.A., Bandettini, P.A., Calhoun, V.D., Corbetta, M., Della Penna, S., Duyn, J.H., Glover, G.H., Gonzalez-Castillo, J., Handwerker, D.A., Keilholz, S., Kiviniemi, V., Leopold, D.A., de Pasquale, F., Sporns, O., Walter, M., Chang, C., et al., 2013. Dynamic functional connectivity: promise, issues, and interpretations. Neuroimage 80, 360–378. doi:10.1016/j.neuroimage.2013.05.079.

Jatoi, M.A., Kamel, N., Malik, A.S., Faye, I., Begum, T., 2014. A survey of methods used for source localization using EEG signals. Biomed. Signal Process. Control 11 (1), 42–52. doi:10.1016/j.bspc.2014.01.009.

Jones, D.T., Knopman, D.S., Gunter, J.L., Graff-Radford, J., Vemuri, P., Boeve, B.F., Petersen, R.C., Weiner, M.W., Jack, C.R., 2016. Cascading network failure across the Alzheimer's disease spectrum. Brain 139 (2), 547–562. doi:10.1093/brain/awv338.

Jones, D.T., Vemuri, P., Murphy, M.C., Gunter, J.L., Senjem, M.L., Machulda, M.M., Przybelski, S.A., Gregg, B.E., Kantarci, K., Knopman, D.S., Boeve, B.F., Petersen, R.C., Jack, C.R., et al., 2012. Non-stationarity in the "resting brain's" modular architecture. PLoS ONE 7 (6). doi:10.1371/journal.pone.0039731.

Khambhati, A.N., Sizemore, A.E., Betzel, R.F., Bassett, D.S., 2018. Modeling and interpreting mesoscale network dynamics. Neuroimage 180 (June), 337–349. doi:10.1016/j.neuroimage.2017.06.029. https://linkinghub.elsevier.com/retrieve/pii/S1053811917305001

Khanna, A., Pascual-Leone, A., Michel, C.M., Farzan, F., 2015. Microstates in resting-state EEG: current status and future directions. Neuroscience &

Biobehavioral Reviews 49, 105–113. doi:10.1016/j.neubiorev.2014.12.010. https://linkinghub.elsevier.com/retrieve/pii/S0149763414003492

Krzakala, F., Moore, C., Mossel, E., Neeman, J., Sly, A., Zdeborova, L., Zhang, P., 2013. Spectral redemption in clustering sparse networks. Proceedings of the National Academy of Sciences 110 (52), 20935–20940. doi:10.1073/pnas.1312486110.

Lai, M., Demuru, M., Hillebrand, A., Fraschini, M., 2018. A comparison between scalp- and source-reconstructed EEG networks. Sci. Rep. 8 (1), 1–8. doi:10.1038/s41598-018-30869-w.

Liuzzi, L., Quinn, A.J., O'Neill, G.C., Woolrich, M.W., Brookes, M.J., Hillebrand, A., Tewarie, P., 2019. How sensitive are conventional MEG functional connectivity metrics with sliding windows to detect genuine fluctuations in dynamic functional connectivity? Front. Neurosci. 13 (JUL), 1–16. doi:10.3389/fnins.2019.00797. https://www.frontiersin.org/article/10.3389/fnins.2019.00797/full

Maestú, F., Yubero, R., Moratti, S., Campo, P., Gil-Gregorio, P., Paul, N., Solesio, E., del Pozo, F., Nevado, A., 2011. Brain activity patterns in stable and progressive mild cognitive impairment during working memory as evidenced by magnetoencephalography. Journal of Clinical Neurophysiology 28 (2), 202–209. doi:10.1097/WNP.0b013e3182121743. http://ovidsp.ovid.com/ovidweb.cgi?T=JS&PAGE=reference&D=emed10&NEWS=N&AN=2011222503 https://insights.ovid.com/crossref?an=00004691-201104000-00013

Marwan, N., Carmen Romano, M., Thiel, M., Kurths, J., 2007. Recurrence plots for the analysis of complex systems. Phys. Rep. 438 (5–6), 237–329. doi:10.1016/j.physrep.2006.11.001.

Mazziotta, J., Toga, A., Evans, A., Fox, P., Lancaster, J., Zilles, K., Woods, R., Paus, T., Simpson, G., Pike, B., Holmes, C., Collins, L., Thompson, P., MacDonald, D., Iacoboni, M., Schormann, T., Amunts, K., Palomero-Gallagher, N., Geyer, S., Parsons, L., Narr, K., Kabani, N., Goualher, G.L., Boomsma, D., Cannon, T., Kawashima, R., Mazoyer, B., 2001. A probabilistic atlas and reference system for the human brain: international consortium for brain mapping (ICBM). Philosophical Transactions of the Royal Society of London. Series B: Biological Sciences 356 (1412), 1293–1322. doi:10.1098/rstb.2001.0915. https://royalsocietypublishing.org/doi/10.1098/rstb.2001.0915

McKhann, G., Knopman, D.S., Chertkow, H., Hymann, B., Jack, C.R., Kawas, C., Klunk, W., Koroshetz, W., Manly, J., Mayeux, R., Mohs, R., Morris, J., Rossor, M., Scheltens, P., Carrillo, M., Weintrub, S., Phelphs, C., et al., 2011. The diagnosis of dementia due to Alzheimer's disease: recommendations from the national institute on aging-Alzheimer's association workgroups on diagnostic guidelines for Alzheimer's disease. Alzheimers Dementia 7 (3), 263–269. doi:10.1016/j.jalz.2011.03.005.The.

Núñez, P., Poza, J., Gómez, C., Barroso-García, V., Maturana-Candelas, A., Tola-Arribas, M.A., Cano, M., Hornero, R., 2020. Characterization of the dynamic behavior of neural activity in Alzheimer's disease: exploring the non-stationarity and recurrence structure of EEG resting-state activity. J. Neural Eng. 17 (1), 016071. doi:10.1088/1741-2552/ab71e9. https://iopscience.iop.org/article/10.1088/1741-2552/ab71e9

Núñez, P., Poza, J., Gómez, C., Rodríguez-González, V., Hillebrand, A., Tola-Arribas, M.A., Cano, M., Hornero, R., 2019. Characterizing the fluctuations of dynamic resting-state electrophysiological functional connectivity: reduced neuronal coupling variability in mild cognitive impairment and dementia due to Alzheimer's disease. J. Neural. Eng. 16 (5), 056030. doi:10.1088/1741-2552/ab234b.

Núñez, P., Poza, J., Gómez, C., Rodríguez-González, V., Hillebrand, A., Tola-Arribas, M.A., Cano, M., Hornero, R., 2019. Characterizing the fluctuations of dynamic resting-state electrophysiological functional connectivity: reduced neuronal coupling variability in mild cognitive impairment and dementia due to Alzheimer's disease. J. Neural Eng. 16 (5), 056030. doi:10.1088/1741-2552/ab234b.

O'Neill, G.C., Barratt, E.L., Hunt, B.a.E., Tewarie, P.K., Brookes, M.J., et al., 2015. Measuring electrophysiological connectivity by power envelope correlation: a technical review on MEG methods. Phys. Med. Biol. 60 (21). doi:10.1088/0031-9155/60/21/R271. R271–R295

O'Neill, G.C., Tewarie, P., Vidaurre, D., Liuzzi, L., Woolrich, M.W., Brookes, M.J., 2018. Dynamics of large-scale electrophysiological networks: a technical review. Neuroimage 180 (May 2017), 559–576. doi:10.1016/j.neuroimage.2017.10.003.

Palop, J.J., Mucke, L., 2010. Amyloid-β-induced neuronal dysfunction in Alzheimer's disease: from synapses toward neural networks. Nat. Neurosci. 13 (7), 812–818. doi:10.1038/nn.2583. http://www.nature.com/articles/nn.2583

Pascual-Marqui, R.D., 2002. Standardized low-resolution brain electromagnetic tomography (sLORETA): technical details. Methods Find Exp Clin Pharmacol 24 (Suppl D), 5–12.

Petersen, R.C., 2004. Mild cognitive impairment as a clinical entity and treatment target. Arch. Neurol. 62 (7), 1160–1163;discussion 1167. doi:10.1001/archneur.62.7.1160.

Pievani, M., de Haan, W., Wu, T., Seeley, W.W., Frisoni, G.B., et al., 2011. Functional network disruption in the degenerative dementias. The Lancet Neurology 10 (9), 829–843. doi:10.1016/S1474-4422(11)70158-2.

Pineda-Pardo, J.A., Bruña, R., Woolrich, M., Marcos, A., Nobre, A.C., Maestú, F., Vidaurre, D., 2014. Guiding functional connectivity estimation by structural connectivity in MEG: an application to discrimination of conditions of mild cognitive impairment. Neuroimage 101, 765–777. doi:10.1016/j.neuroimage.2014.08.002.

Ponce-Alvarez, A., Deco, G., Hagmann, P., Romani, G.L., Mantini, D., Corbetta, M., 2015. Resting-State temporal synchronization networks emerge from connectivity topology and heterogeneity. PLoS Comput. Biol. 11 (2), e1004100. doi:10.1371/journal.pcbi.1004100.

Poza, J., Gómez, C., García, M., Tola-Arribas, M.A., Carreres, A., Cano, M., Hornero, R., et al., 2017. Spatio-Temporal fluctuations of neural dynamics in mild cognitive impairment and Alzheimer's disease. Curr. Alzheimer Res. 14 (9), 924–936. doi:10.2174/1567205014666170309115656. http://www.eurekaselect.com/150776/article

Prichard, D., Theiler, J., 1994. Generating surrogate data for time series with several simultaneously measured variables. Phys. Rev. Lett. 73 (7), 951–954.

Ramirez-Mahaluf, J.P., Medel, V., Tepper, A., Alliende, L.M., Sato, J.R., Ossandon, T., Crossley, N.A., 2020. Transitions between human functional brain networks reveal complex, cost-efficient and behaviorally-relevant temporal paths. Neuroimage 117027. doi:10.1016/j.neuroimage.2020.117027. https://linkinghub.elsevier.com/retrieve/pii/S1053811920305139

Rodríguez-González, V., Gómez, C., Shigihara, Y., Hoshi, H., Hornero, R., Revilla, M., Poza, J., 2020. Consistency of local activation parameters at sensor- and source-level in neural signals. J. Neural Eng. doi:10.1088/1741-2552/abb582.

Rossini, P.M., Di Iorio, R., Vecchio, F., Anfossi, M., Babiloni, C., Bozzali, M., Bruni, A.C., Cappa, S.F., Escudero, J., Fraga, F.J., Giannakopoulos, P., Guntekin, B., Logroscino, G., Marra, C., Miraglia, F., Panza, F., Tecchio, F., Pascual-Leone, A., Dubois, B., 2020. Early diagnosis of Alzheimer's disease: the role of biomarkers including advanced EEG signal analysis. report from the IFCN-sponsored panel of experts. Clinical Neurophysiology 131 (6), 1287–1310. doi:10.1016/j.clinph.2020.03.003.

Rubinov, M., Sporns, O., 2010. Complex network measures of brain connectivity: uses and interpretations. Neuroimage 52 (3), 1059–1069. doi:10.1016/j.neuroimage.2009.10.003.

Rubinov, M., Sporns, O., 2011. Weight-conserving characterization of complex functional brain networks. Neuroimage 56 (4), 2068–2079. doi:10.1016/j.neuroimage.2011.03.069.

Schumacher, J., Peraza, L.R., Firbank, M., Thomas, A.J., Kaiser, M., Gallagher, P., O'Brien, J.T., Blamire, A.M., Taylor, J.-P., 2019. Dynamic functional connectivity changes in dementia with lewy bodies and Alzheimer's disease. NeuroImage: Clinical 22 (August 2018), 101812. doi:10.1016/j.nicl.2019.101812. https://linkinghub.elsevier.com/retrieve/pii/S2213158219301627

Sitnikova, T.A., Hughes, J.W., Ahlfors, S.P., Woolrich, M.W., Salat, D.H., 2018. Short timescale abnormalities in the states of spontaneous synchrony in the functional neural networks in Alzheimer's disease. NeuroImage: Clinical 20 (May), 128–152. doi:10.1016/j.nicl.2018.05.028. https://linkinghub.elsevier.com/retrieve/pii/S2213158218301748

Tadel, F., Baillet, S., Mosher, J.C., Pantazis, D., Leahy, R.M., 2011. Brainstorm: A User-Friendly application for MEG/EEG analysis. Comput Intell Neurosci 2011, 1–13. doi:10.1155/2011/879716.

Tewarie, P., Liuzzi, L., O'Neill, G.C., Quinn, A.J., Griffa, A., Woolrich, M.W., Stam, C.J., Hillebrand, A., Brookes, M.J., 2019. Tracking dynamic brain networks using high temporal resolution MEG measures of functional connectivity. Neuroimage 200 (June), 38–50. doi:10.1016/j.neuroimage.2019.06.006. https://linkinghub.elsevier.com/retrieve/pii/S1053811919304914

Theiler, J., Eubank, S., Longtin, A., Galdrikian, B., Doyne Farmer, J., 1992. Testing for nonlinearity in time series: the method of surrogate data. Physica D 58 (1–4), 77–94. doi:10.1016/0167-2789(92)90102-S.

Tognoli, E., Kelso, J.A.S., 2014. The metastable brain. Neuron 81 (1), 35–48. doi:10.1016/j.neuron.2013.12.022. https://linkinghub.elsevier.com/retrieve/pii/S0896627313011835

Vidaurre, D., Hunt, L.T., Quinn, A.J., Hunt, B.A.E., Brookes, M.J., Nobre, A.C., Woolrich, M.W., 2018. Spontaneous cortical activity transiently organises into frequency specific phase-coupling networks. Nat. Commun. 9 (1), 2987. doi:10.1038/s41467-018-05316-z.

Vidaurre, D., Llera, A., Smith, S.M., Woolrich, M.W., 2019. Behavioural relevance of spontaneous, transient brain network interactions in fMRI. bioRxiv doi:10.1101/779736.

Vidaurre, D., Quinn, A.J., Baker, A.P., Dupret, D., Tejero-Cantero, A., Woolrich, M.W., 2016. Spectrally resolved fast transient brain states in electrophysiological data. Neuroimage 126, 81–95. doi:10.1016/j.neuroimage.2015.11.047.

Vidaurre, D., Smith, S.M., Woolrich, M.W., 2017. Brain network dynamics are hierarchically organized in time. Proceedings of the National Academy of Sciences 114 (48), 12827–12832. doi:10.1073/pnas.1705120114.

Vohryzek, J., Deco, G., Cessac, B., Kringelbach, M.L., Cabral, J., 2020. Ghost attractors in spontaneous brain activity: recurrent excursions into functionally-Relevant BOLD phase-Locking states. Front. Syst. Neurosci. 14 (April), 1–15. doi:10.3389/fnsys.2020.00020. https://www.frontiersin.org/article/10.3389/fnsys.2020.00020/full

Webber, C.L., Zbilut, J.P., 2005. Recurrence quantification analysis of nonlinear dynamical systems. Tutorials in contemporary nonlinear methods for the Behavioral Sciences Web Book 26–94. https://www.nsf.gov/sbe/bcs/pac/nmbs/chap2.pdf

Xia, M., Wang, J., He, Y., 2013. Brainnet viewer: A Network visualization tool for human brain connectomics. PLoS ONE 8 (7). doi:10.1371/journal.pone.0068910.

Zalesky, A., Fornito, A., Cocchi, L., Gollo, L.L., Breakspear, M., 2014. Time-resolved resting-state brain networks. Proceedings of the National Academy of Sciences 111 (28), 10341–10346. doi:10.1073/pnas.1400181111.

Zhou, Q., Zhang, L., Feng, J., Lo, C.-Y.Z., 2019. Tracking the main states of dynamic functional connectivity in resting state. Front. Neurosci. 13 (JUL), 1–12. doi:10.3389/fnins.2019.00685. https://www.frontiersin.org/article/10.3389/fnins.2019.00685/full

Zhuang, X., Yang, Z., Mishra, V., Sreenivasan, K., Bernick, C., Cordes, D., 2020. Single-scale time-dependent window-sizes in sliding-window dynamic functional connectivity analysis: a validation study. Neuroimage 220 (April), 117111. doi:10.1016/j.neuroimage.2020.117111.